

Regime Transitions of Cross-Equatorial Hadley Circulations with Zonally Asymmetric Thermal Forcings

JUN ZHAI AND WILLIAM BOOS

Department of Geology and Geophysics, Yale University, New Haven, Connecticut

(Manuscript received 15 January 2015, in final form 20 May 2015)

ABSTRACT

Observed nonlinearities in the seasonal evolution of monsoons have been previously explained using theories for Hadley circulations driven by zonally symmetric thermal forcings, even though monsoonal forcings deviate strongly from the assumption of zonal symmetry. Here, an idealized model of a dry, three-dimensional atmosphere is used to compare the response to zonally symmetric and asymmetric off-equatorial thermal forcings. For symmetric forcings, the zonal-mean, cross-equatorial mass flux increases more rapidly with the amplitude of the forcing once the forcing becomes strong enough to reduce the upper-tropospheric absolute vorticity to near zero, consistent with previous studies of the transition to angular momentum-conserving flow. For zonally asymmetric forcings, the zonal-mean cross-equatorial flow exhibits a similar dependence on forcing strength and a similar reduction of the zonal-mean upper-level vorticity, but asymmetric forcings also produce strong zonal overturnings with subsidence west of the heating, as in the well-known linear response to off-equatorial heatings. The mass flux in these zonal overturnings increases linearly with forcing strength until its rate of increase tapers off for the strongest forcings; the total upward mass flux (i.e., the zonal-mean plus zonally asymmetric components) increases linearly with the strength of zonally asymmetric forcings and exhibits no abrupt or nonlinear dependence on forcing amplitude. These results indicate the importance of considering the zonally asymmetric part of the divergent response to off-equatorial forcings and suggest that theories based on zonally symmetric forcings need further examination before they can be assumed to describe observed monsoons.

1. Introduction

Monsoon circulations consist of highly three-dimensional flow forced by heat sources localized in regions with irregular coastlines and topography. Nevertheless, it has become common to describe monsoons as zonally symmetric meridional overturning circulations with precipitating ascent in the summer hemisphere, cross-equatorial flow, and subsidence in the winter hemisphere (Webster and Fasullo 2003). Monsoon circulations do, indeed, project strongly onto the zonal-mean Hadley circulation during solstice seasons, with most cross-equatorial mass flux in the Hadley circulation composed of flow through monsoon regions (e.g., Peixoto and Oort 1992; Findlater 1969; Boos and Emanuel 2009). While it is not obvious that a highly three-dimensional circulation can be

adequately described in terms of zonal-mean quantities, even when the zonal-averaging operator is applied over a limited range of longitudes, abstracting monsoons as zonal-mean circulations has facilitated much study of monsoon dynamics.

In the past 30 years, multiple theoretical advances made in understanding Earth's Hadley circulation have been extended to solstice-like conditions representative of monsoons. Held and Hou (1980) developed an axisymmetric¹ theory for the strength and meridional extent of the annual-mean Hadley circulation, and Lindzen and Hou (1988) extended this theory to cross-equatorial flow driven by off-equatorial thermal forcings. Central to this axisymmetric theory is the idea that meridional flow

Corresponding author address: Jun Zhai, Department of Geology and Geophysics, Yale University, 210 Whitney Avenue, New Haven, CT 06511.
E-mail: jun.zhai@yale.edu

¹Consistent with the literature discussed herein, we use “axisymmetric” to refer to circulations that have no variations about the planetary rotation axis. While “axisymmetric” can be a synonym for “zonally symmetric,” we will use the latter term to describe a thermal forcing that is invariant with longitude in order to be clear that we are not assuming the resulting circulation is axisymmetric.

conserves absolute angular momentum about Earth's rotational axis, a constraint that leads to a nonlinear dependence of circulation strength on parameters such as the strength and meridional structure of the thermal forcing.

When an off-equatorial thermal forcing is confined to the subtropics, [Plumb and Hou \(1992\)](#) showed that an axisymmetric, angular momentum conserving (AMC) meridional circulation will exist only if the forcing exceeds a critical amplitude. This results from a steady, inviscid form of the axisymmetric zonal momentum balance:

$$(f + \zeta)v = 0 \quad (1)$$

where f is the Coriolis parameter, v is the meridional wind, and ζ is the vertical component of relative vorticity. If the geostrophically balanced zonal flow produced by the thermal forcing is not strong enough to reduce the absolute vorticity to zero, then (1) shows that v must be zero. In the presence of viscosity and friction, nonzero v occurs for such subcritical forcings but intensifies nonlinearly once the forcing exceeds the threshold where $f + \zeta \simeq 0$. This theoretical explanation for the nonlinear dependence of a cross-equatorial circulation on its forcing was compelling, because the South Asian summer monsoon is observed to intensify more rapidly than can be explained by a linear response to the insolation forcing (e.g., [Yin 1949](#); [Krishnamurti et al. 1981](#); [Murakami et al. 1986](#)). Although [Plumb and Hou \(1992\)](#) used a dry, highly idealized numerical model in their work, subsequent studies showed that nonlinear transitions of axisymmetric, AMC circulations also occur in moist models with steady off-equatorial forcings ([Emanuel 1995](#); [Zheng and Eltahir 1998](#); [Privé and Plumb 2007a](#)) and with time-varying off-equatorial forcings ([Boos and Emanuel 2008a,b](#)).

The axisymmetric theory of Hadley flow discussed above assumes that absolute angular momentum is homogenized in the free troposphere by the zonal-mean meridional wind and neglects, in the domain of the Hadley circulation, momentum transports by zonally asymmetric eddies. The annual-mean observed Hadley circulation has since been shown to deviate from such a state of uniform absolute angular momentum, and momentum transports by baroclinic eddies have been shown to be central to the dynamics of the Hadley circulation ([Walker and Schneider 2005, 2006](#)). In particular, the strength and extent of the annual-mean and equinox Hadley circulations have been shown to scale with the divergence of meridional eddy momentum fluxes in a series of idealized general circulation models [GCMs; see review by [Schneider \(2006\)](#)]. In other words, a dominant term in the time-mean, zonal-mean, zonal momentum balance is the eddy momentum flux divergence S :

$$(f + [\bar{\zeta}])[\bar{v}] \simeq S, \quad (2)$$

where brackets denote a zonal mean and an overbar denotes a time mean. Nonzero $[\bar{v}]$ can thus exist for nonzero absolute vorticities because the right-hand side of (2) is nonzero.

While the observed annual-mean Hadley circulation is thus not well described by the axisymmetric, AMC theory of [Held and Hou \(1980\)](#), the cross-equatorial Hadley circulation in boreal summer does lie closer to the AMC limit, particularly in the longitudes of the South Asian monsoon ([Schneider and Bordoni 2008](#)). However, even if the AMC theory could be applied to the mean summer state of the South Asian monsoon, the transition between the equinox and solstice states cannot be exactly that described by [Plumb and Hou \(1992\)](#), because baroclinic eddy momentum fluxes, rather than linear viscosity, are a central part of the circulation dynamics for subcritical off-equatorial thermal forcings. [Walker and Schneider \(2006\)](#) and [Schneider and Bordoni \(2008\)](#) used dry idealized GCMs with zonally symmetric thermal forcings to show that the transition between equinox and solstice states seems to be between a weak equinox regime in which eddy-momentum fluxes control the strength of Hadley flow {i.e., S and $f + [\bar{\zeta}]$ in (2) are both nonzero} and a strong solstice regime in which meridional flow is only weakly influenced by eddy fluxes (i.e., S and $f + [\bar{\zeta}]$ are each near zero). The transition between the two regimes is abrupt (i.e., circulation strength increases nonlinearly with the latitude of the peak thermal forcing) and occurs robustly in idealized moist GCMs with time-varying thermal forcings ([Bordoni and Schneider 2008](#)). Thus, it seems reasonable to assert that the abrupt onset of the South Asian summer monsoon might occur because of a transition from an eddy-dominated regime to an axisymmetric-like AMC regime.

However, all of the Hadley circulation theories discussed above assume zonally symmetric forcings, whether or not they allow for the transport of momentum by transient, zonally asymmetric eddies. Observed monsoon flows are produced by thermal forcings with large zonal asymmetries, as evidenced by the strong zonal asymmetry in upper-tropospheric temperature and absolute vorticity observed in the Asian summer monsoon ([Fig. 1](#)). Linear theory for the steady response to an off-equatorial, zonally confined heat source has long served as a useful tool for understanding the observed zonally asymmetric distribution of winds and rain in monsoons, as in the highly influential papers by [Gill \(1980\)](#) and [Hoskins and Rodwell \(1995\)](#). But [Plumb \(2007\)](#) noted that it is difficult to reconcile such linear theory for the response to a zonally asymmetric forcing with the nonlinear theories for zonal-mean Hadley flow

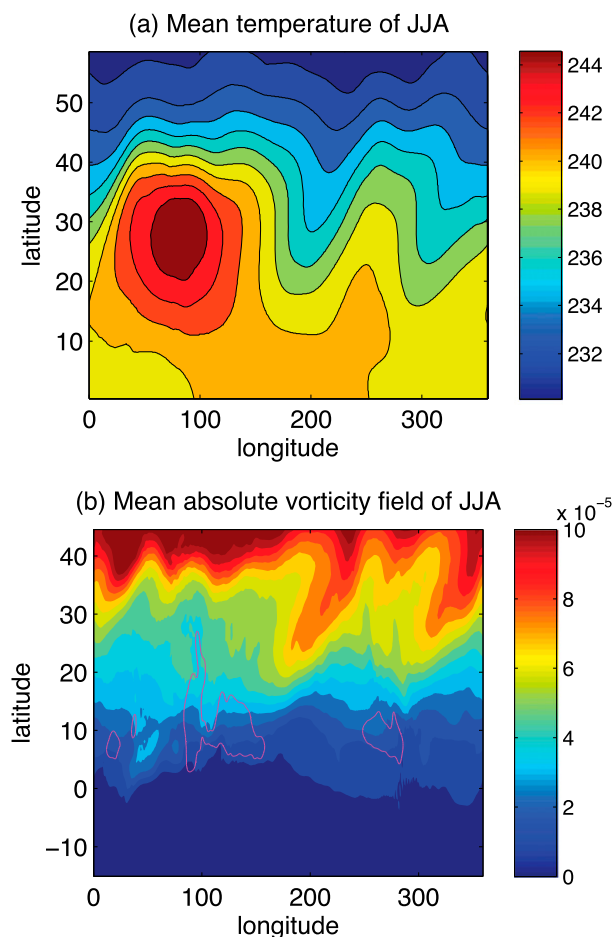


FIG. 1. Illustration of strong zonal asymmetry of the boreal summer (June–August) mean state: (a) 200–400-hPa temperature (K) and (b) absolute vorticity at 250 hPa (color shading) and vertical velocity at 300 hPa (magenta lines). All data are from ERA-Interim (ECMWF 2010) and averaged from 1979 to 2010. The vertical velocity isolines in (b) mark 30% of the maximum magnitude of upward motion, spatially smoothed six times with a 1–2–1 filter.

described by either Held and Hou (1980) or Walker and Schneider (2006).

Some reconciliation lies in explorations of the nonlinear response to zonally asymmetric thermal forcings, which show that the condition of uniform absolute angular momentum generalizes to a condition of zero absolute vorticity in regions of divergent upper-tropospheric flow (Schneider 1987). More precisely, integration of the inviscid momentum equation around a closed contour having a particular absolute vorticity η provides a constraint on the time-mean divergent flow, as described by Hsu and Plumb (2000) and reviewed by Plumb (2007):

$$\eta \iint_A \nabla \cdot \bar{\mathbf{u}} dA = - \iint_A \nabla \cdot (\overline{\eta \mathbf{u}'}) dA. \quad (3)$$

Here, primes represent deviations from the time mean and A is the area enclosed by a contour of constant η . The integral on the left-hand side represents the net mass flux across the chosen η contour, while the right-hand side represents the transient eddy flux of vorticity across the contour. If the flow is steady and there is no transient eddy flux, a thermal forcing can produce a divergent circulation only if $\eta = 0$ in the region of divergent flow. However, regions of near-zero η produced by zonally asymmetric heatings on rotating spheres are known to become dynamically unstable, spreading westward from the source in an anticyclonic β plume that periodically breaks down into low-vorticity eddies that propagate away from the source region (Rhines 1983; Hsu and Plumb 2000). These transients provide a vorticity flux into the region of the heating that allows the time-mean η to remain nonzero even while there is divergent flow. Regions of low-potential vorticity air have been observed to break off from the Asian summer monsoon anticyclone and propagate westward (Popovic and Plumb 2001). Sobel and Plumb (1999) showed that the transient vorticity fluxes vanish in (3) if the integral is taken over a contour that is allowed to deform in time, and any time-mean net mass flux across the contour must be balanced by viscous effects. Viscous effects become more important as transient eddies stretch the vorticity field into fine filaments with sharp horizontal gradients (Plumb 2007).

An open issue is how the strength of the divergent response to an off-equatorial, zonally confined thermal forcing varies with the strength of that forcing. In other words, as the strength of a zonally asymmetric heating is increased, does the shedding of low-vorticity air from the heating region alter the rate at which the divergent circulation strengthens? Or can scalings developed for zonally symmetric forcings (e.g., Walker and Schneider 2006) be applied even though the time-mean response will contain large zonal asymmetries? Our hypothesis is that the divergent mass flux produced by a zonally asymmetric heating will not exhibit the abrupt, nonlinear transitions seen in the response to a zonally symmetric heating, because the eddy flux of vorticity into the heating region will prevent the circulation from achieving the nonlinear, zero-vorticity state. Even if the absolute vorticity becomes small enough to produce nonlinear flow, we hypothesize that eddy activity will reduce the rapidity with which the transition to the AMC state occurs.

The influence of thermal forcing asymmetries on cross-equatorial monsoon circulations was previously examined by Privé and Plumb (2007b), but they focused on other aspects of the moist response and did not examine how the meridional circulation scaled with the

strength of a zonally asymmetric forcing. Shaw (2014) analyzed the role played by planetary-scale waves in the onset of the boreal summer general circulation and did examine how the circulation changed as a wavenumber-2 thermal perturbation was increased in amplitude relative to a zonally symmetric basic state. Once the wavenumber-2 forcing in her model exceeded a threshold, the circulation transitioned to a state dominated by stationary waves and anticyclonic absolute vorticity in the equatorial upper troposphere in some longitudes. This change in sign of the absolute vorticity occurred as part of a southward migration of negative relative vorticity from the Northern Hemisphere as the stationary wave amplitude was increased (T. A. Shaw 2015, personal communication) and is distinct from the regime transitions marked by absolute vorticity reaching zero in the region of the off-equatorial heating (e.g., Plumb and Hou 1992; Hsu and Plumb 2000). Nevertheless, the results of Shaw (2014), as well as those of Kelly and Mapes (2011, 2013), illustrate the important role played by stationary eddy momentum transports in the boreal summer general circulation. This study is complementary to that work in that we also force an idealized model with a zonally asymmetric thermal forcing, but here we focus on the scaling of the total vertical mass flux, integrated over all longitudes, instead of just the zonal mean.

One particular goal of this paper is to examine how both the zonally symmetric and asymmetric parts of the divergent response vary with the strength of the forcing. When Privé and Plumb (2007b) examined the response to heating from a zonally asymmetric continent, they noted that much of the ascent that occurred over the off-equatorial continent was accompanied by subsidence to the west-northwest, which is qualitatively consistent with the linear response to a zonally confined heating (e.g., Gill 1980). We know of no study that clearly shows how the total vertical mass flux (zonally symmetric and asymmetric components) produced by an off-equatorial heating varies with the amplitude of that heating. This question is presumably highly relevant to the seasonal evolution of precipitation in monsoons, because that precipitation will increase with the total ascent, not just its zonally symmetric component.

The forcings used in this study are all confined to off-equatorial regions and vary only in amplitude, retaining a constant spatial structure similar to that used in Plumb and Hou (1992). This contrasts with the approach of Walker and Schneider (2006) and Schneider and Bordoni (2008), who examined the transition between equinox and solstice states by moving the peak of the equilibrium temperature distribution from the equator into the subtropics. While we eventually wish to examine the effect of forcing asymmetries in such a configuration, as it is likely

more relevant to real monsoon circulations with cross-equatorial SST gradients, addition of zonal asymmetries to the Plumb–Hou-type forcing seems more straightforward as a first step. All forcings are applied in a dry, idealized GCM by relaxing the temperature toward a prescribed equilibrium distribution. The effects of moisture, time variations in the forcing, and other complications will be explored in future work.

The next section of this paper provides details on our numerical model and further information on the forcing. Results are then presented, and we close with a summary and discussion of caveats and implications.

2. Model setup

We used the finite-volume dynamical core of the Community Atmosphere Model, version 5.0 (CAM5.0), developed by the National Center for Atmospheric Research (NCAR; Neale et al. 2012). We used a resolution of 1.9° latitude by 2.5° longitude, with 30 vertical levels from the surface pressure of about 1000 hPa to the model top near 0 hPa. A few integrations were conducted at a finer resolution, as described in the results section below. There is no moisture or topography.

The model circulation is forced by a scheme very similar to that described by Held and Suarez (1994), which employs linear relaxation of temperatures toward a prescribed equilibrium distribution over a time scale of 40 days throughout most of the troposphere. We modified the equilibrium temperature distribution as described below, but all other aspects of the forcing are as described in Held and Suarez (1994). For example, boundary layer dissipation is represented by linear relaxation of winds toward zero in the lowest 30% of the atmosphere's mass. We used a 30-min time step with the model state output as 6-hourly averages. All output was transformed to pressure coordinates for analysis.

We conducted two sets of integrations: one forced by zonally symmetric equilibrium temperature profiles and the other by zonally asymmetric equilibrium temperatures. All integrations used time-invariant equilibrium temperature distributions and were run for 10 years with the last 9 years used for analysis.

a. Zonally symmetric forcing

We prescribed an equilibrium temperature distribution T_e with a meridional structure identical to that used by Plumb and Hou (1992):

$$T_e(\lambda, \varphi, \sigma) = \frac{\pi}{2} A_e F(\lambda) \sin\left(\pi \frac{1-\sigma}{0.8}\right) \Phi(\varphi) + T_0(\sigma), \quad (4)$$

where

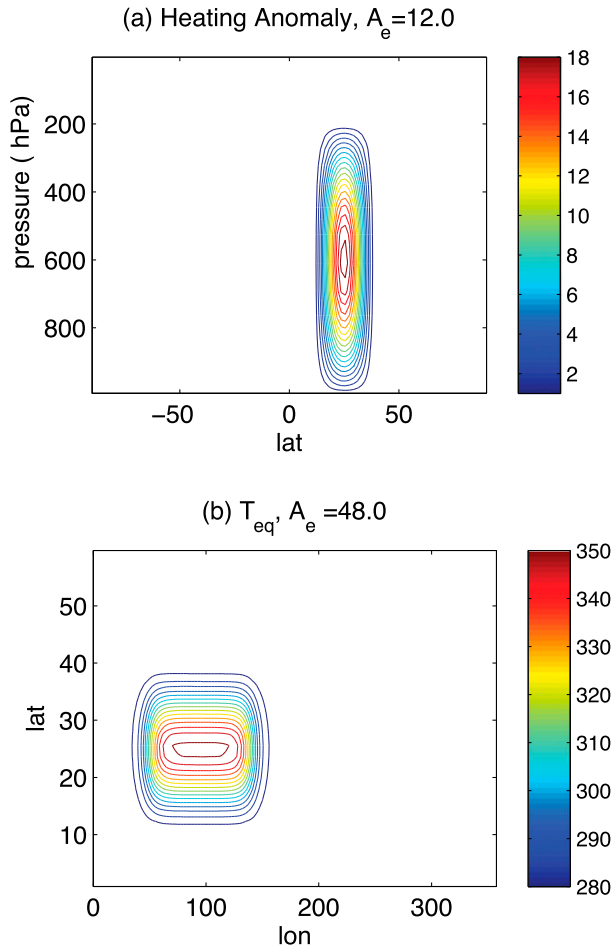


FIG. 2. (a) Zonal-mean equilibrium temperature T_e anomaly (K), relative to the horizontally uniform background, for zonally symmetric forcing with $A_e = 12$ K. Contour interval is 1 K. (b) Total equilibrium temperature T_e (K) at 600 hPa for zonally asymmetric forcing with $A_e = 48$ K. Contour interval is 5 K, starting at 280 K.

$$\Phi(\varphi) = \begin{cases} \cos^2\left(\frac{\pi}{2} \frac{\varphi - \varphi_0}{\Delta\varphi}\right), & \text{if } \varphi_0 - \Delta\varphi \leq \varphi \leq \varphi_0 + \Delta\varphi \\ 0, & \text{otherwise} \end{cases} \quad (5)$$

Here, $\sigma = p/p_s$ where p_s is surface pressure, and T_e is set to T_0 for all $\sigma < 0.2$. The function $F(\lambda)$ allows for the introduction of zonal asymmetries in T_e and is equal to unity for all zonally symmetric forcings. As shown in Fig. 2a, the peak T_e is centered on $\varphi_0 = 25^\circ\text{N}$ and has a meridional half-width of $\Delta\varphi = 15^\circ$. The constant A_e represents the amplitude of the equilibrium temperature anomaly, which peaks in the midtroposphere and has a maximum of $\pi A_e/2$ relative to the background T_0 . We conducted a series of integrations in which A_e varied from 0 to 13.5 K with an increment of 1.5 K (but was

constant in time in each integration). The background T_0 is the same stably stratified profile used on the equator in Held and Suarez (1994), and here we omit any meridional temperature gradient in T_0 .

b. Zonally asymmetric forcing

In a second set of integrations, we used a zonally confined, purely off-equatorial forcing as an idealization of the heating produced by an off-equatorial continent spanning a limited range of longitudes (e.g., Asia or Australia). Cross-equatorial sea surface temperature (SST) gradients and baroclinicity in the winter extratropics may indeed play a role in monsoon circulations but are not considered here. We modified T_e by confining the maximum equilibrium temperature anomaly to one quarter of each latitude circle. To avoid introducing zonal discontinuities in T_e , we smoothed the edges of this zonally asymmetric equilibrium temperature maximum using a hyperbolic tangent. This was all accomplished by introducing the function $F(\lambda)$ in (4):

$$F(\lambda) = \frac{1}{2} \tanh\left(\frac{\lambda - \lambda_1}{\Delta\lambda}\right) - \frac{1}{2} \tanh\left(\frac{\lambda - \lambda_2}{\Delta\lambda}\right), \quad (6)$$

where λ is longitude (radians), the zonal boundaries of the T_e maximum are λ_1 and λ_2 , and $\Delta\lambda$ is the zonal scale over which the edges of this maximum are smoothed. Here, $\lambda_1 = 5\pi/18$, $\lambda_2 = 14\pi/18$, and $\Delta\lambda = \pi/18$. This confines the equilibrium temperature maximum between about 50° and 140°E longitude in the Northern Hemisphere, which is approximately the domain of the Asian continent. The horizontal structure of the zonally asymmetric T_e is illustrated in Fig. 2b. Because the T_e maximum only occupies one-quarter of the planetary circumference (or more precisely, because $2\pi/\int_0^{2\pi} F d\lambda = 4$), we will often compare the response to a zonally symmetric forcing of strength A_e with the response to a zonally asymmetric forcing of strength $4A_e$. Thus, the set of integrations conducted with zonally asymmetric forcings used values of A_e ranging from 0 to 54 K in increments of 6 K.

3. Results

We first present an analysis of the zonal-mean circulation resulting from both the zonally symmetric and zonally asymmetric forcings. Then we examine how the total vertical mass flux, including its zonally asymmetric component, scales with the strength of the forcing. Finally, we analyze the upper-tropospheric vorticity budget in order to explore the relevance of transitions to AMC states.

a. Spatial structure of the circulation

For both weak and strong zonally symmetric forcings, the zonal-mean circulation consists of three cells: a thermally

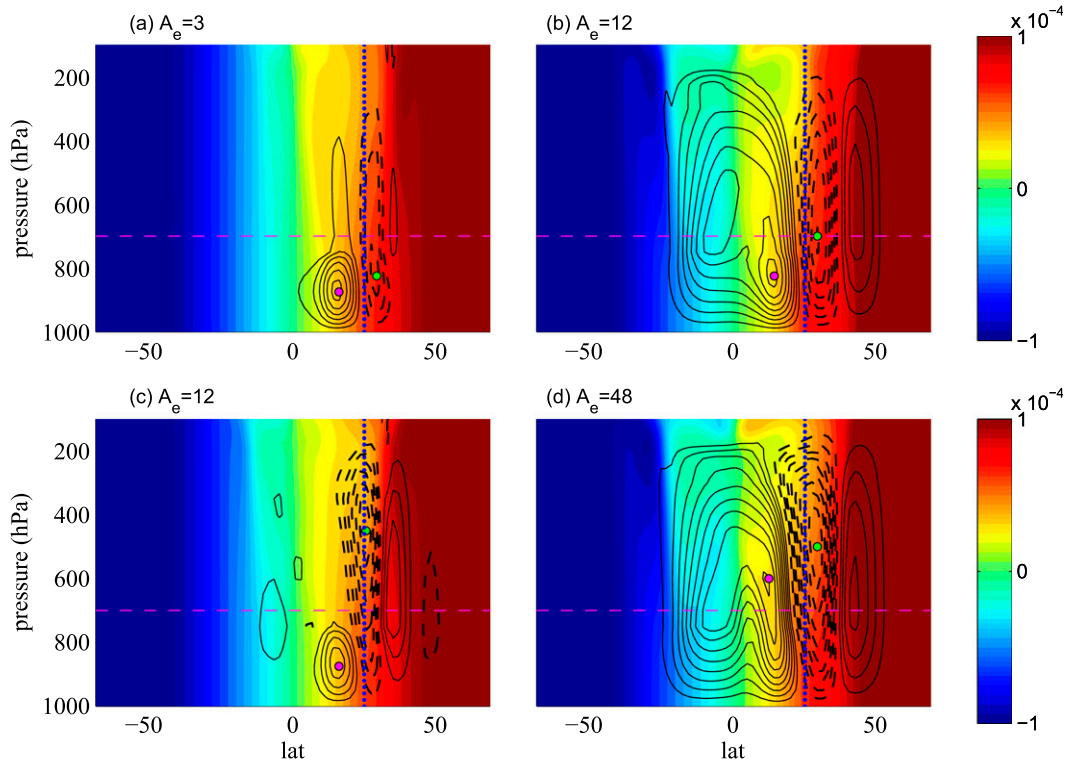


FIG. 3. Time-mean, zonal-mean distributions of mass streamfunction (black contours) and absolute vorticity (color shading; s^{-1}) for weak and strong forcings: (a) zonally symmetric forcing with $A_e = 3$ K (weak forcing), (b) zonally symmetric forcing with $A_e = 12$ K (strong forcing), (c) zonally asymmetric forcing with $A_e = 12$ K (weak forcing), and (d) zonally asymmetric forcing with $A_e = 48$ K (strong forcing). For mass streamfunction, solid lines represent counterclockwise flow and dashed lines represent clockwise flow. Streamfunction contour interval is (a),(c) 1 Sverdrup ($1 \text{ Sv} = 10^6 \text{ m}^3 \text{ s}^{-1}$) for weak forcings and (b),(d) 5 Sv for strong forcings, with the zero contour omitted. Contour interval for absolute vorticity is $5 \times 10^{-6} \text{ s}^{-1}$. The magenta dot marks the streamfunction extremum Ψ_{max} in the winter cell (from 30°S to 30°N), and the green dot marks the streamfunction extremum in the summer cell (from 20° to 40°N). The horizontal magenta dashed line marks the top of the boundary layer, and the vertical blue dashed line marks the latitude of the T_e maximum.

direct tropical cell that for strong forcings crosses the equator, a subtropical cell that is also thermally direct, and a thermally indirect cell centered near 40°N (Figs. 3a,b). The last of these corresponds to Earth's Ferrel cell, while the first two are qualitatively similar to the observed boreal summer Hadley circulation and so are referred to herein as the winter and summer cells, respectively. For the weakest forcings (e.g., $A_e = 3$ K), the winter cell is confined almost entirely within the boundary layer and within the region where meridional gradients of T_e are nonzero, which suggests that this circulation consists simply of linear, viscous flow. Indeed, the northward and southward boundary layer flow occurs in regions of eastward and westward flow, respectively (Fig. 4), consistent with a zonal-mean zonal momentum balance between linear drag and $f v$. This is consistent with the idea that weak forcings can produce meridional flow only in regions with mechanical damping, which in our model are confined entirely below 700 hPa. The absolute

vorticity field deviates little from its resting state (i.e., $\eta \simeq f$) for these weak forcings, confirming that the circulation is in a linear regime far from the AMC limit (e.g., Held and Hou 1980; Plumb and Hou 1992).

The meridional and vertical scales of the winter cell increase greatly as the amplitude of the zonally symmetric forcing is increased so that, for strong forcings, it extends through the full depth of the troposphere and encompasses the entirety of the tropical belt in both hemispheres (e.g., Figure 3b). The circulation is strong enough to homogenize the absolute angular momentum field and create a region of low absolute vorticity in much of the tropical upper troposphere, indicating that these strongly forced circulations are in a nonlinear, AMC regime. The cross-equatorial flow seen for strong forcings exhibits an equatorial jump similar in appearance to that discussed by Pauluis (2004), so it is presumably caused by boundary layer friction and the absence of strong cross-equatorial gradients in the T_e

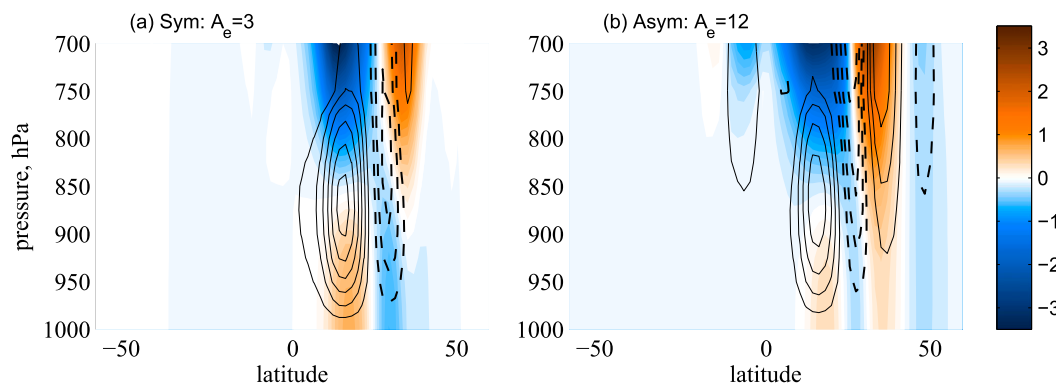


FIG. 4. Time-mean boundary layer zonal-mean zonal wind (m s^{-1} ; color shading) and zonal-mean mass streamfunction (Sv; black contours) for (a) zonally symmetric ($A_e = 3$ K) and (b) zonally asymmetric ($A_e = 12$ K) weak forcings. Streamfunction contour intervals are as in Fig. 3.

distribution. Compared to Earth's observed solstitial Hadley circulation (e.g., Dima and Wallace 2003), the summer cell and Ferrel cell are too strong, presumably because we prescribed an equilibrium temperature profile that has an overly strong meridional temperature gradient in the Northern Hemisphere's extratropics. This deviation from observations will be revisited below; we emphasize that we are not attempting to realistically simulate Earth's Hadley circulation but to examine some of the dynamics resulting from the breaking of zonal symmetry of the forcing.

Now we examine the zonal-mean circulation that results from the zonally asymmetric forcings. For weak forcings, we expect the zonal-mean response to depend only on the zonal-mean T_e , but stationary wave momentum fluxes may modify the response to strong forcings (as they did in Shaw 2014). Nevertheless, we find that the zonal-mean forcing approximately determines the zonal-mean response even for strong forcings. The zonal-mean response to zonally asymmetric forcings with $A_e = 12$ and 48 K closely resembles the zonal-mean response to symmetric forcings with $A_e = 3$ and 12 K, respectively (Fig. 3; recall that A_e for the zonally asymmetric forcing must be 4 times as large as for the symmetric forcing to achieve the same zonal-mean T_e distribution). The weak asymmetric forcing does produce a stronger summer cell and a stronger Ferrel cell than the weak symmetric forcing and also has an additional thermally direct cell poleward of the Ferrel cell that is absent for the symmetric forcing. For the strongest forcings, each circulation cell is stronger for the asymmetric forcing, but only by 10%–40%. The equatorial jump is also more prominent for the strong asymmetric forcing than for the strong symmetric forcing, and the streamfunction maximum of the winter cell is positioned at a higher altitude. Otherwise, the zonal-mean circulations are quite similar for the two types of

forcing, with all strong forcings producing low zonal-mean absolute vorticity throughout the tropical upper troposphere.

It is not surprising that the zonally asymmetric forcings produce stronger circulations for the same zonal-mean T_e distribution, because asymmetric forcings induce stationary waves that flux zonal momentum meridionally. To quantify the effect of eddy activity on the zonal-mean flow, we computed the stationary and transient components of the horizontal eddy momentum flux convergence (HEMFC). For the strong zonally symmetric forcing, transient HEMFC peaks in the upper troposphere and opposes the Coriolis torque produced by the upper-level mean meridional circulation in the Ferrel and summer cells (Fig. 5b). The strong asymmetric forcing has a qualitatively similar distribution of transient HEMFC in the upper troposphere, but its transient HEMFC is weaker and is accompanied by stationary HEMFC of similar magnitude (Figs. 5d and 6b). The total HEMFC produced by the asymmetric forcing is of higher amplitude, consistent with the stronger summer and Ferrel cells produced by that forcing. The zonally asymmetric forcing also produces strong transient and stationary HEMFC in the lower troposphere in the region of the peak T_e (i.e., between 10° and 40°N). Although the transient HEMFC produced by the weak forcings has such a small amplitude that it is not visible on the scale used in Fig. 5, the weak asymmetric forcing produces a substantial stationary HEMFC that seems to balance the stronger summer and Ferrel cells produced by that forcing. The stationary HEMFC produced by the zonally symmetric forcings is not shown because it is so small.

The above zonal-mean view masks large differences between the circulations produced by the zonally symmetric and asymmetric forcings. For weak forcings, both symmetric and asymmetric forcings produce zonal-mean ascent near the T_e maximum at 25°N, but the asymmetric

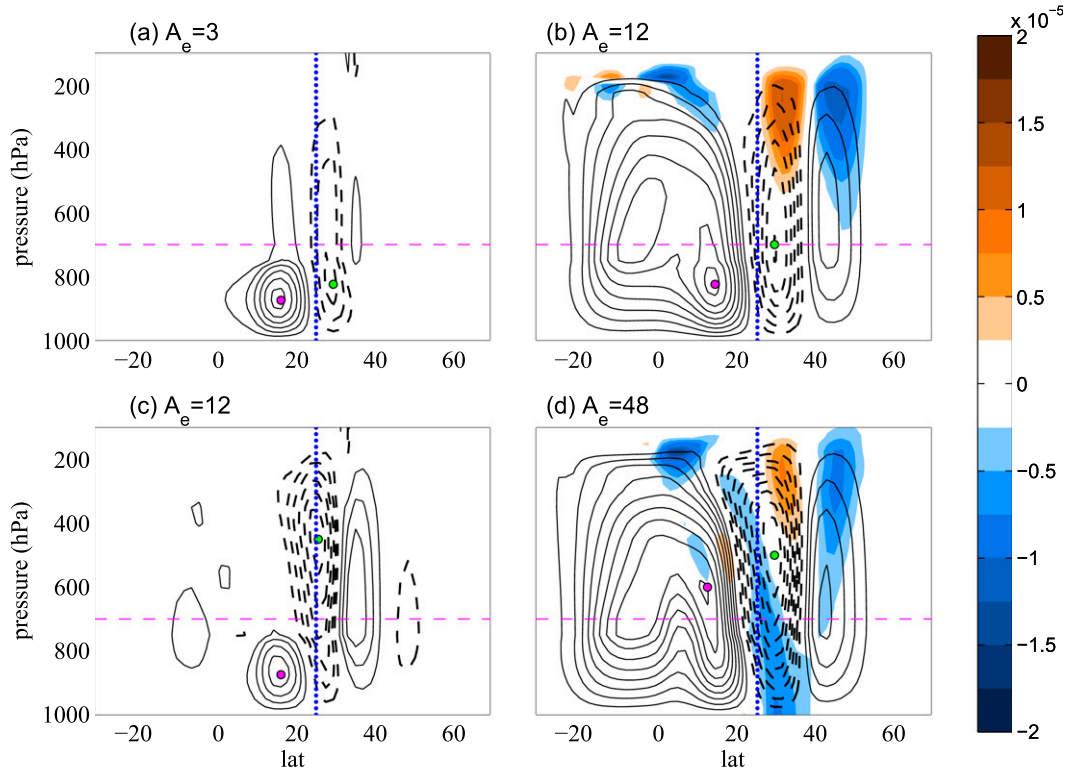


FIG. 5. As in Fig. 3, but with colors showing the divergence of horizontal transient eddy momentum flux (m s^{-2}), with values of magnitude less than 10% of the maximum not shown.

forcing produces maximum ascent near 30°N , 140°E , near the eastern edge of the T_e maximum and in a latitude of zonal-mean subsidence (Figs. 7a,c). Subsidence lies to the west of this zonally asymmetric ascent, and the zonal dipole in vertical velocity is located on the edges of an upper-level anticyclone centered over the T_e maximum. This dynamical pattern is quite familiar from linear solutions for the response to an imposed off-equatorial heating (Webster 1972; Gill 1980).

The response to the strong asymmetric forcing also exhibits many of these features, although changes in spatial structure suggest the presence of at least some nonlinearity (Fig. 7d). Compared to the response to the weak asymmetric forcing, the peak ascent is located farther toward the equator, near 20°N at a latitude of zonal-mean ascent rather than zonal-mean subsidence. The peak subsidence is shifted poleward together with the westerly branch of the upper-tropospheric anticyclone. Thus, we expect less cancellation of ascent and subsidence when the zonal mean is taken than we saw in the case of the weak forcing. We also expect the response to the strong forcing to lie closer to the zonally asymmetric AMC limit in which nonlinear meridional advection of zonal momentum becomes important; this is consistent with the fact that we no longer find the

linear Sverdrup vorticity balance with ascent and subsidence on the eastern and western sides of the upper-tropospheric anticyclone.

b. Mass flux scaling

To study how circulation strength changes with forcing amplitude, we examine several measures of the mass flux in the time-mean overturning circulation. The first index, Ψ_{\max} , is the maximum meridional mass streamfunction from 30°S to 30°N , which is a conventional measure of the strength of the Hadley circulation used by many previous authors (e.g., Plumb and Hou 1992; Schneider and Bordoni 2008). This index represents the total mass flux in the cross-equatorial cell of the Eulerian zonal-mean meridional overturning circulation. For a given zonal-mean T_e distribution, both zonally symmetric and zonally asymmetric forcings produce similar values of Ψ_{\max} , with the circulation intensifying more rapidly as a function of A_e for $A_e \geq 7\text{ K}$ (or $A_e/4 \geq 7\text{ K}$ for asymmetric forcings; Fig. 8; note the change in vertical scale between panels). This is consistent with the general similarities in the zonal-mean streamfunctions seen in the top and bottom rows of Fig. 3, and suggests that a regime transition in the zonal-mean circulation might occur for both symmetric and asymmetric forcings at this value of A_e .

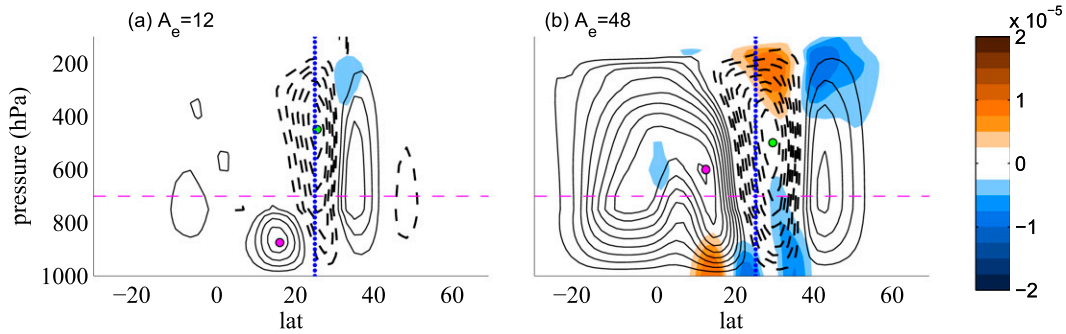


FIG. 6. As in Fig. 3, but with colors showing the divergence of horizontal stationary eddy momentum flux (m s^{-2}) for zonally asymmetric (a) weak and (b) strong forcings, with values of a magnitude less than 10% of the maximum not shown.

We now examine a second index of circulation strength: a zonal and meridional integral of the upward vertical velocity, which provides a measure of the vertical mass flux contained in meridional overturnings as well as in zonal overturnings that would average to zero in a zonal mean. This integral is evaluated at 700 hPa, the top of the boundary layer in which velocities are linearly damped. We would ideally like the lateral boundaries of

this integral to include thermally direct ascent in the Hadley circulation but to exclude thermally indirect ascent in the Ferrel cell, as well as ascent in the equatorial jump (e.g., Fig. 3d). For the zonally symmetric forcing, this is accomplished by integrating the vertical velocity at 700 hPa ω_{700} from the latitude of maximum ascent southward and northward to the latitudes ϕ^- and ϕ^+ at which the ascent decays to zero:

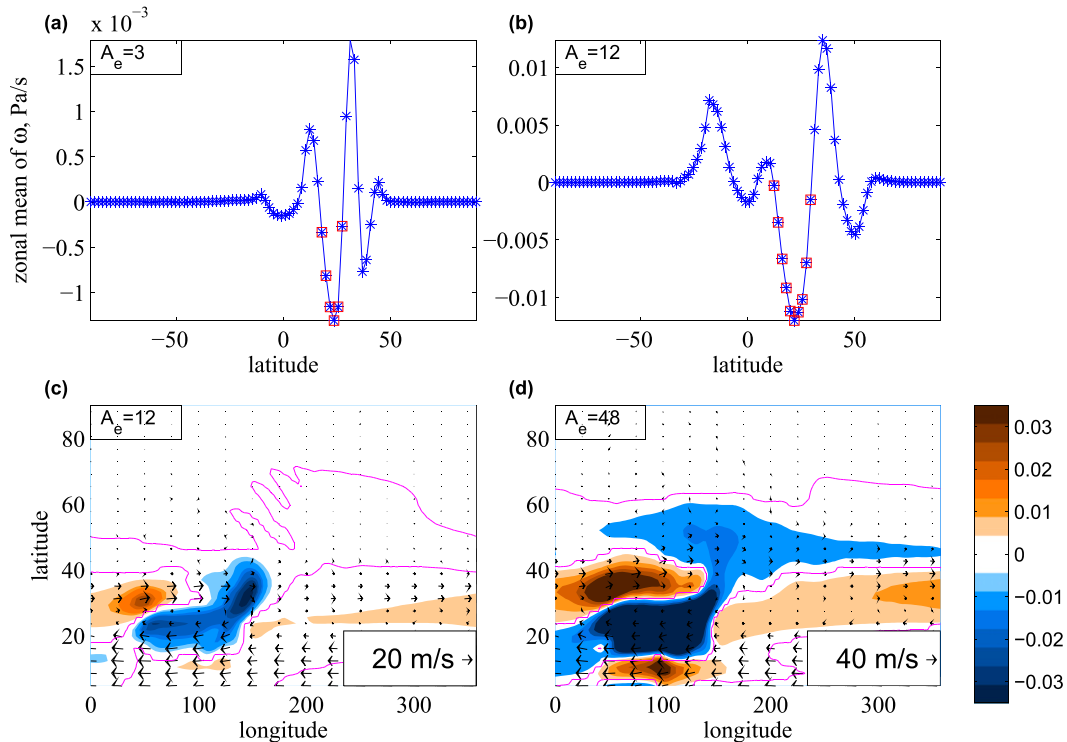


FIG. 7. (top) Zonal-mean vertical velocity (Pa s^{-1}) at 700 hPa for (a) weak ($A_e = 3 \text{ K}$) and (b) strong ($A_e = 12 \text{ K}$) zonally symmetric forcings. The red squares mark the points included in integration of the ascending mass flux at 700 hPa W_{sym} , defined by (7). (bottom) Time-mean winds for (c) weak ($A_e = 12 \text{ K}$) and (d) strong ($A_e = 48 \text{ K}$) zonally asymmetric forcings. Color shading shows vertical velocity (Pa s^{-1}) at 700 hPa, vectors show horizontal winds at 200 hPa, and the magenta contour marks zero vertical velocity.

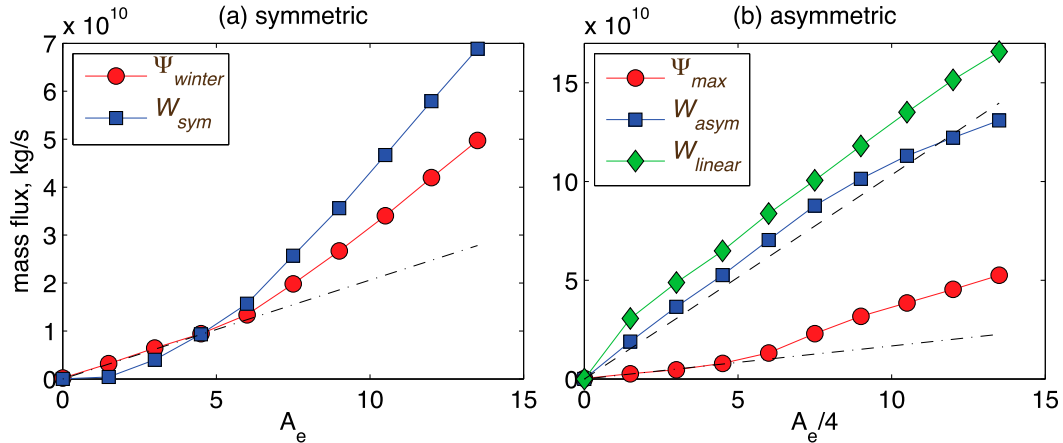


FIG. 8. Dependence of mass flux indices on forcing strength for (a) symmetric and (b) asymmetric forcings (kg s^{-1}). The red lines are the streamfunction maxima of the winter cells (from 30°S to 30°N), and the blue lines are the vertical ascending mass flux defined in (7) and (8). The black dashed–dotted lines show an approximate linear scaling for Ψ_{max} . In (b), the green line is the quasi-linear approximation for the mass flux given in (11), and the black dashed line is the same approximation but using a spatially invariant stratification equal to twice that in the unforced model (see text for details).

$$W_{\text{sym}} \equiv -\frac{R^2}{g} \int_0^{2\pi} \int_{\phi^-}^{\phi^+} \omega_{700} \cos(\phi) \, d\phi \, d\lambda. \quad (7)$$

By construction, this integral represents the total upward mass flux at 700 hPa contained in the winter and summer Hadley cells. The integrated vertical mass flux W_{sym} is smaller than Ψ_{max} for weak forcings (Fig. 8a) because the streamfunction extremum is located in the boundary layer below 700 hPa (Fig. 3a). For strong zonally symmetric forcings, W_{sym} is larger than Ψ_{max} because it includes the ascent in the summer Hadley cell (i.e., the clockwise cell positioned between 20° and 40°N in Fig. 3b). Since most theoretical studies of the strength of Hadley circulations have relied on an index like Ψ_{max} that measures only the component of ascent associated with the cross-equatorial cell (e.g., Plumb and Hou 1992), it is useful to have an alternate measure of the total ascent occurring in the Hadley circulation. Overall, though, Ψ_{max} and W_{sym} exhibit qualitatively similar behavior as the strength of the zonally symmetric forcing is increased; W_{sym} has a larger curvature for weak forcings, but both indices intensify more rapidly as a function of A_e once A_e exceeds about 7 K.

For asymmetric forcings, choosing the limits of integration for the vertical mass flux index is more difficult because there is no clear boundary between ascent in the Hadley and Ferrel cells. For example, for a weak asymmetric forcing, zonal-mean ascent occurs in Hadley cells near 20°N and in the Ferrel cell near 40°N (Fig. 3c), but, in plan view, an elongated band of intense ascent can be seen stretching between these two latitude bands (Fig. 7c). So, when spatially integrating the upward mass

flux, we first use limits that simply include all ascending regions in most of the Northern Hemisphere, excluding only the area within 5° of the equator to eliminate ascent in the equatorial jump:

$$W_{\text{asym}} \equiv \frac{R^2}{g} \int_0^{2\pi} \int_{\pi/36}^{\pi/2} \omega_{700} \mathcal{H}(-\omega_{700}) \cos(\phi) \, d\phi \, d\lambda. \quad (8)$$

Here, \mathcal{H} is the Heaviside function. To be clear, this and all other vertical mass flux indices are calculated using time-mean vertical velocities averaged over 9 years. A “gross upward mass flux” (e.g., Schneider et al. 2010) obtained by sampling upward vertical velocities on near-daily time scales would presumably be much larger and subject to different constraints. The integral W_{sym} has a much larger amplitude than Ψ_{max} for all values of the asymmetric forcing (Fig. 8b). It exhibits no nonlinear increase in sensitivity to A_e but, instead, increases linearly for weak-to-moderate forcings and has a weaker rate of increase for the strongest forcings.

Part of the increased mass flux measured by W_{asym} compared to Ψ_{max} occurs in the thermally indirect Ferrel cell. To find whether this thermally indirect ascent is responsible for the different scaling behavior of W_{asym} and Ψ_{max} , we construct another mass flux index that includes only thermally direct ascent:

$$W_{\text{direct}} \equiv -\frac{R^2}{g} \int_0^{2\pi} \int_{\pi/36}^{\pi/2} \omega_{700} \mathcal{H}(-\omega' T'_{700}) \mathcal{H}(-\omega_{700}) \cos(\phi) \, d\phi \, d\lambda. \quad (9)$$

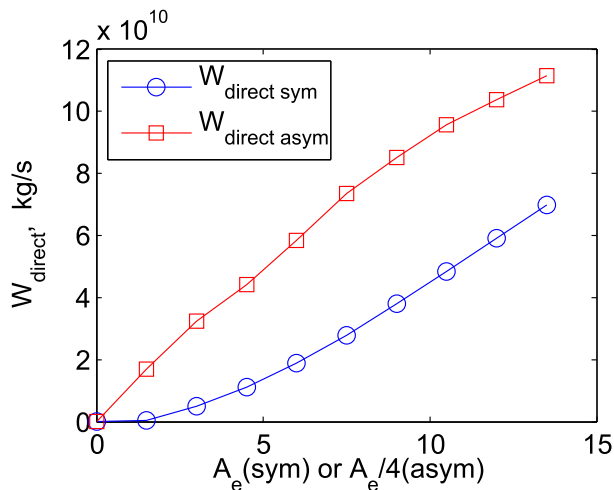


FIG. 9. Thermally direct ascending mass flux calculated using (9). The blue line is for zonally symmetric forcings, and the red line is for zonally asymmetric forcings.

Here, ω' and T' are time-mean anomalies relative to the global-mean values of those variables on the 700-hPa pressure surface, and $\omega = \omega'$ because mass is conserved. For the symmetric forcing, W_{direct} behaves similarly to the mass flux in the ascending branches of the Hadley cell represented by W_{sym} , intensifying more rapidly as a function of A_e as A_e increases past 5–7 K (Fig. 9). For the asymmetric forcing, W_{direct} does not exhibit an increase in sensitivity as the forcing strength increases and, like W_{asym} , decreases in sensitivity to A_e for the strongest forcings. It is remarkable that, for a given zonal-mean T_e distribution, the thermally direct mass flux produced by the asymmetric forcing is as much as several times stronger than that produced by the symmetric forcing. Including the thermally indirect Ferrel cell ascent in the indices shown in Fig. 8 thus made little difference in the overall scaling behavior. Thus, the zonal-mean mass streamfunction greatly underestimates the total vertical mass flux produced by asymmetric thermal forcings.

We examine one other index to estimate the strength of the summer Hadley cell: the absolute value of the minimum (i.e., the most negative) zonal-mean mass streamfunction value between 20° and 50°N, denoted by Ψ_{min} . This index scales nonlinearly for both symmetric and asymmetric forcings, with Ψ_{min} increasing more rapidly once A_e (or $A_e/4$ for asymmetric forcings) exceeds 2–3 K (Fig. 10). This nonlinearity is stronger for the asymmetric forcing: the summer cell produced by the asymmetric forcing is almost twice as strong as that produced by the symmetric forcing, consistent with the larger stationary eddy momentum fluxes produced by asymmetric forcings. Thus, the linear scaling of total

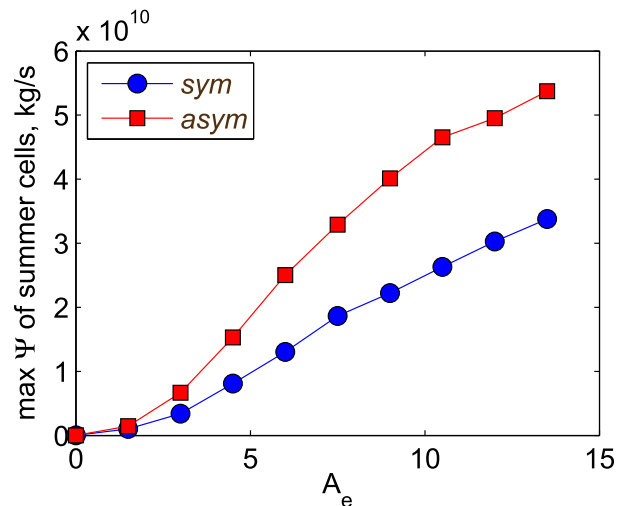


FIG. 10. The maximum magnitude of the zonal-mean mass streamfunction (kg s^{-1}) in the summer cells (from 20° to 50°N). The blue line is for zonally symmetric forcings, and the red line is for zonally asymmetric forcings.

ascent seen for asymmetric forcings is not caused by the summer cell compensating for the nonlinear increase of the winter cell. Both the summer and winter cells have intensities that increase nonlinearly with the amplitude of the zonally asymmetric forcing, so it must be the zonally asymmetric circulation that produces the near-linear dependence of the total mass flux on forcing amplitude.

We also applied (7) to the zonally asymmetric component of the vertical velocity field (i.e., $\omega - [\omega]$). As shown in Fig. 11, the sensitivity of the zonally asymmetric part of the vertical mass flux W_{prime} to the forcing decreases as the forcing strength increases. This compensates for the nonlinear increase in sensitivity in the zonal-mean circulation Ψ_{max} to produce a near-linear dependence of the total mass flux on A_e . We also calculated the thermally direct part of the zonally asymmetric ascending mass flux using (9), and that quantity exhibited a similar scaling trend to W_{prime} (not shown).

Finally, we compare the response to asymmetric forcings with a simple quasi-linear scaling. Our GCM is forced by relaxing temperatures toward the prescribed equilibrium distribution T_e , but this forcing (i.e., the right-hand side of the thermodynamic equation) can instead be written as the combination of a prescribed heating rate and a linear damping like that used in the linear model of Gill (1980):

$$-\frac{1}{\tau}(T - T_e) = Q - \frac{T}{\tau}, \quad (10)$$

with the heating rate $Q = T_e/\tau$ and $\tau = 40$ days throughout most of the troposphere.² Assuming a weak temperature gradient approximation (Sobel and Bretherton 2000), in which Q is balanced

entirely by adiabatic cooling in the ascending branch of the circulation, allows the vertical mass flux to be expressed as a linear function of the forcing amplitude A_e :

$$W_{\text{WTG}} = -A_e \left[\frac{\pi R^2}{2\tau} \sin\left(\pi \frac{1-\sigma}{0.8}\right) \right] \int_0^{2\pi} \int_{\pi/36}^{\pi/2} \frac{F(\lambda)\Phi(\varphi)}{\mathcal{S}} \cos(\phi) d\phi d\lambda. \quad (11)$$

The coefficients in this expression depend on the invariant horizontal structure of the forcing given by $\Phi(\varphi)$ and $F(\lambda)$ as defined in (5) and (6). Strict linearity is compromised by the fact that the stratification $\mathcal{S} = gT\partial_p \ln\theta$ can and does vary with forcing amplitude, increasing by roughly a factor of 2 with some spatial variability as A_e increases by a factor of 10. Furthermore, (11) neglects the effect of the thermal damping in (10), which we estimate to be on the order of 20% of Q . We therefore present two quantities: a calculation of W_{WTG} using the actual stratification diagnosed from each model integration (green line in Fig. 8b), and a true linear scaling obtained by using twice the stratification of the unforced integration as \mathcal{S} (dashed line in Fig. 8b). The total upward vertical mass flux produced by asymmetric forcings W_{asym} is approximately described by either of these scalings, indicating that the circulation exhibits a near-linear response to the forcing after changes to the stratification are taken into account. The increase in stratification likely explains some of the decreased sensitivity of the zonally asymmetric mass flux to A_e seen at high values of A_e . Although the stratification changes might be viewed as an artifact of the lack of a convective constraint on temperature profiles, the stratification would also increase as temperatures warm in a moist convecting atmosphere.

In summary, the zonal-mean response to both symmetric and asymmetric forcings becomes more sensitive to the forcing once A_e and $A_e/4$, respectively, reach about 7 K. This sort of nonlinear response is seen in both the winter and summer Hadley cells and in the total zonal-mean ascent at 700 hPa (the W_{sym} index). Asymmetric forcings produce an asymmetric circulation that makes no contribution to the zonal-mean flow but that is stronger than the zonal-mean flow. The total upward mass flux, integrated over all longitudes and latitudes,

increases linearly with the strength of the asymmetric forcing and exhibits no abrupt increase in sensitivity to the forcing. In fact, the sensitivity of this total upward mass flux to the forcing decreases for very strong forcings. This is true even if one excludes thermally indirect ascent such as occurs in the Ferrel cell.

c. Upper-level vorticity distribution

Several questions naturally arise regarding the response to our forcings. First, is the abrupt increase in sensitivity of the zonal-mean mass flux to the forcing that occurs near $A_e \simeq 7$ K associated with a transition to an AMC state? Second, why does the total upward mass flux produced by the asymmetric forcing scale linearly with A_e , even though the zonal-mean response to the asymmetric forcing seems to undergo some sort of nonlinear transition near $A_e/4 \simeq 7$ K? To answer these questions, we examine the local vertical component of the upper-tropospheric absolute vorticity η .

We find the minimum value of η within a three-dimensional volume spanning the equilibrium temperature maximum (10°–40°N, 40°–160°E, and 175–250 hPa) and plot this as a function of the forcing amplitude A_e . No zonal mean is taken when evaluating the minimum η , since a zonally asymmetric forcing can achieve a zero vorticity state locally even though the zonal-mean circulation is far from this limit. Since the local T_e maximum is the relevant forcing for the local η distribution, we refrain from normalizing A_e by the usual factor of 4 for the asymmetric forcings.

For the symmetric forcing, upper-tropospheric η in the heating region decreases sharply as the strength of the forcing is increased (Fig. 12a). While it does not reach zero, it does approach that limit for the strongest forcings, which produce a local minimum of η near 15°N (Fig. 12b). When η nears its lowest values, the zonal-mean mass flux in the cross-equatorial Hadley cell increases more rapidly with the strength of the forcing, as evidenced by the fact that the change in slope of the red line in Fig. 8 occurs when the minimum η drops to about $1.8 \times 10^{-5} \text{ s}^{-1}$. This value of η , which is found near 15°N, corresponds to a local Rossby number $R_o = -\zeta/f \simeq 0.5$. Walker and Schneider (2006) found similar values of R_o

² When expressed in this manner, the peak amplitude of Q ranges from 0 to 2 K day⁻¹ for our asymmetric forcings. Since this forcing is applied over a region having a horizontal scale of thousands of kilometers, and since the Held–Suarez model has a stratification that is typically weaker than that of a moist adiabatic atmosphere, the largest forcing is quite strong.

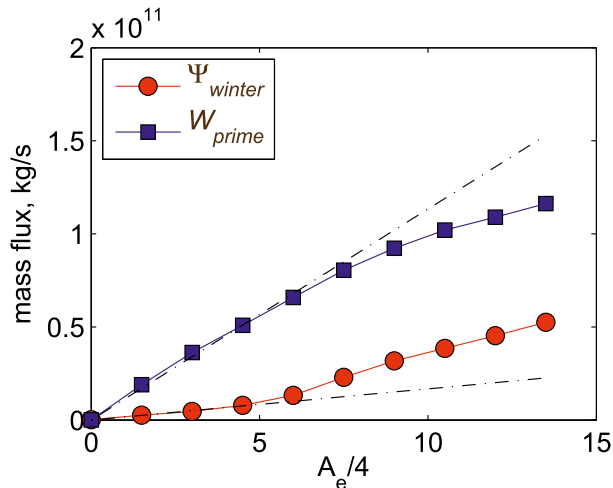


FIG. 11. The streamfunction maxima of the winter cells (red line), and the vertical ascending mass flux in the zonally asymmetric component of the circulation (blue line), all for zonally asymmetric forcings. The blue line (W_{prime}) was calculated by applying (8) to the zonally asymmetric component of vertical velocity. The black dashed-dotted lines show approximate linear scalings. The red line is identical to that shown in Fig. 8b.

when their idealized zonal-mean, cross-equatorial Hadley circulations underwent a regime transition to an approximate AMC state, indicating that the increase in sensitivity of Ψ_{max} that occurs near $A_e \approx 7$ K is indeed associated with a transition to an AMC state. Note that, for the weakest symmetric forcings, the minimum η in our three-dimensional volume is larger than the minimum value of f in that volume. This occurs because the circulation response is local to the forcing and exports η from the center

of the heating region to its periphery (e.g., red line in Fig. 12b).

For asymmetric forcings, Fig. 12a shows that the minimum value of η decreases much more slowly with A_e than for the symmetric forcings so that a much stronger local forcing is needed to produce the same local values of η . The zonal-mean value of T_e seems to be relevant here, as the minimum value of η drops below $2 \times 10^{-5} \text{ s}^{-1}$ for a symmetric forcing with $A_e = 6$ K and an asymmetric forcing with $A_e = 24$ K. In contrast, even the weakest asymmetric forcing produces a maximum R_o of about 0.5. For the asymmetric forcings, the minimum value of η occurs on the equatorial edge of our control volume, where zonal asymmetries in η are small, while the maximum R_o occurs near 25°N in the region of maximum T_e , where zonal asymmetries in winds are large (not shown). Asymmetric forcings thus do not create a local minimum of η near the T_e maximum, and although they produce high values of R_o in longitudes local to the peak forcing, these local R_o values are not associated with a transition in the zonal-mean circulation strength. Although R_o values are locally elevated in the subtropics where the asymmetric part of the vertical mass flux is strong, they seem to be sufficiently localized and far enough from the $R_o = 1$ limit to allow a linear scaling for the mass flux to approximate the response (as shown in Fig. 8).

What process prevents the subtropical circulation from achieving a low-vorticity state in response to strong asymmetric forcings? Hsu and Plumb (2000) showed that strong asymmetric forcings can produce a dynamically unstable upper-level anticyclone that periodically

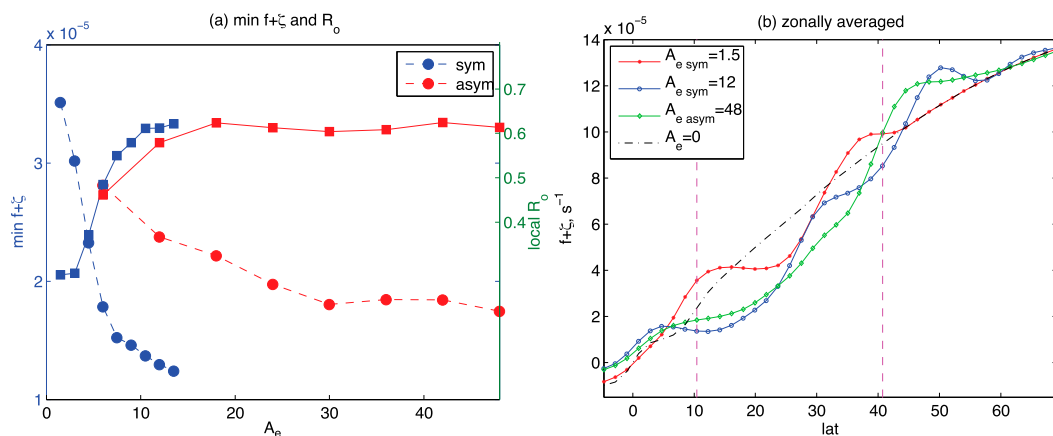


FIG. 12. (a) Minimum absolute vorticity (dashed lines with circles; s^{-1}) and maximum local Rossby number $R_o = -\zeta/f$ (solid lines with squares) in the region $175\text{--}250$ hPa, $10^\circ\text{--}40^\circ\text{N}$, $40^\circ\text{--}160^\circ\text{E}$, and for different forcing strengths. Blue lines are for zonally symmetric forcing, and red lines are for zonally asymmetric forcing. (b) Zonal-mean absolute vorticity for zonally symmetric forcings with $A_e = 1.5$ (red lines) and $A_e = 12$ K (blue lines) and for the zonally asymmetric forcing with $A_e = 48$ K (green lines). The Coriolis parameter is shown as the black dashed-dotted line for reference. The vertical dashed lines are the latitudes (10° and 40°N) between which the extrema of absolute vorticity and R_o in (a) are selected.

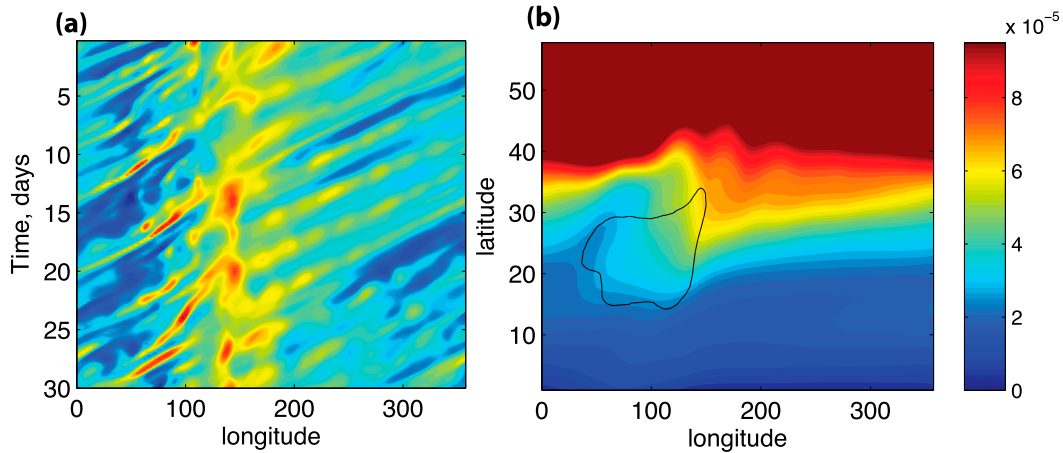


FIG. 13. (a) Hovmöller diagram of absolute vorticity (s^{-1}) at 200 hPa and 25°N for asymmetric forcing with $A_e = 48\text{ K}$. (b) Time-mean absolute vorticity (s^{-1}) at 200 hPa for asymmetric forcing with $A_e = 48\text{ K}$. The black contour marks upward vertical velocity with 30% of the magnitude of the global maximum upward motion.

sheds low-vorticity air. This sort of transient behavior is readily seen in our model in response to strong asymmetric forcings: a Hovmöller diagram of η at 200 hPa shows low-vorticity air generated around the heating center (near 95°E) then propagating westward and being replaced by high-vorticity air in a cycle that recurs about every 10 days (Fig. 13a). The amplitude of these temporal variations is large, with η at 25°N in the heating region varying in time between values that typically only occur at 40°N and at the equator in the time-mean state (Fig. 13b). However, examination of the vorticity budget in the next section will show that the associated transient eddy fluxes of vorticity make a relatively small contribution to the vorticity budget in this region.

d. Upper-level vorticity budget

We showed in the previous section that, while both symmetric and asymmetric thermal forcings reduce η substantially below f , it still has a locally cyclonic value in regions of upper-level divergence that necessitates an eddy flux of vorticity. Here, we examine the time-mean vorticity budget to better understand the nature of these eddy fluxes. We start with the flux form of the inviscid vorticity equation (e.g., Haynes and McIntyre 1987) but separate the term involving the advective flux of vorticity into terms representing horizontal advection and stretching by the time-mean flow and by transient eddies:

$$\frac{\partial \bar{\zeta}}{\partial t} = -\bar{\mathbf{u}} \cdot \nabla \bar{\eta} - \bar{\eta} \nabla \cdot \bar{\mathbf{u}} - \nabla \cdot (\bar{\mathbf{u}}' \eta') + \nabla \cdot \left(\omega \hat{\mathbf{k}} \times \frac{\partial \bar{\mathbf{u}}}{\partial p} \right). \quad (12)$$

The first two terms on the right-hand side represent horizontal advection of vorticity and vortex stretching

by the time-mean flow, respectively. The third term represents convergence of the horizontal advective flux of vorticity by transient eddies, which is computed explicitly from 6-h-averaged data. The last term, which is the sum of the tilting and vertical advection terms for the total flow (mean plus transient eddies), is omitted from the plots presented below because it is comparatively small in the upper troposphere for all forcings examined here. We also calculate a budget residual, neglecting the Eulerian time tendency in our 9-yr averages, as the sum of all the terms on the right-hand side of (12).

For strong symmetric forcings, the upper-level vorticity budget behaves as expected for a Hadley circulation approaching the AMC limit. The symmetric thermal forcing produces ascent near 25°N , which in turn produces a negative vorticity tendency through the stretching term (i.e., vortex squashing; Fig. 14). In the AMC limit, this tendency would be zero because $\bar{\eta}$ would be zero, but in our model $\bar{\eta}$ is nonzero, and the negative stretching tendency is balanced by convergence of the transient eddy flux of vorticity. Advection by the time-mean flow produces a negative tendency in the heating region because time-mean flow diverges out of a local vorticity minimum. The vorticity budget poleward of 30°N behaves generally as expected, with upper-level vortex stretching in the downward and upward branches of the Ferrel cell balanced by transient eddy activity. The budget residual in the region of the heating is just as large as the stretching term but is considerably smaller than other terms in the subsiding region near 40°N . Although the magnitude of this residual might seem large at first consideration, as the circulation approaches the AMC limit, the stretching and advective terms will approach zero, and thus any budget residual will be large in

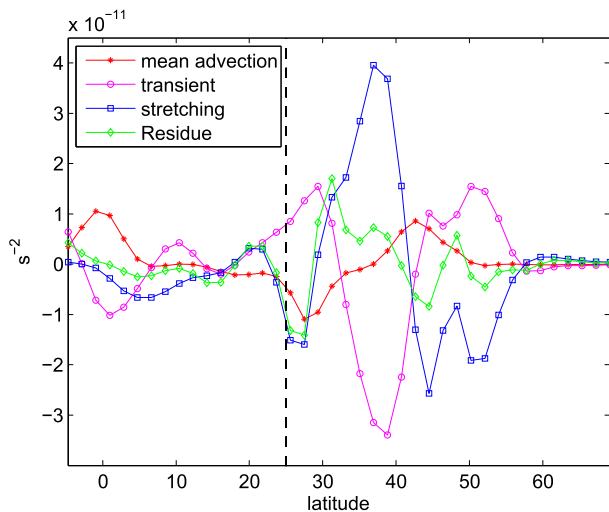


FIG. 14. Zonal-mean components of the vorticity budget, as in (12), at 200 hPa for zonally symmetric forcing with $A_e = 12$ K. All components have units of s^{-2} . Individual lines show horizontal advection of absolute vorticity by the time-mean flow ($-\bar{\mathbf{u}} \cdot \nabla \bar{\eta}$; mean advection), the sum of transient terms ($-\mathbf{u}' \cdot \nabla \eta' - \eta' \nabla \cdot \mathbf{u}'$; transient), and vortex stretching by the mean flow ($-\bar{\eta} \nabla \cdot \bar{\mathbf{u}}$; stretching). The sum of all of the above plus vertical advection and tilting terms [i.e., $\nabla \cdot [\omega \hat{\mathbf{k}} \times (\partial \mathbf{u} / \partial p)]$] is marked “residue.” The vertical dashed line marks the location of the equilibrium temperature maximum.

comparison. We did repeat the integration shown in Fig. 14 with the horizontal grid spacing reduced by a factor of 2 and found that the budget residual dropped by about 30% in magnitude for most latitudes (not shown), indicating that numerical effects may make some contribution to the budget residual. Although there is no explicit diffusion in the model at 200 hPa, the finite-volume dynamical core of CAM5.0 employs a monotonicity constraint that can mix strongly via an implicit nonlinear diffusion, and the effects of this are difficult to assess (Neale et al. 2012).

For asymmetric forcings, the negative tendency due to vortex stretching in the heating region reaches values that are about an order of magnitude larger than for the symmetric forcing. This is true for both weak (Fig. 15) and strong asymmetric forcings (Fig. 16), and the fact that the stretching tendency increases with A_e is consistent with the fact that these asymmetric forcings produce a circulation far from the $\eta \approx 0$ limit. The large (negative) vortex stretching by the time-mean flow is balanced primarily by horizontal vorticity advection by the mean flow, with the effects of transient eddies remaining comparatively small. These mean advective tendencies are positive on the eastern edge of the upper-level anticyclone, where equatorward flow advects large planetary vorticity toward the equator, and negative in the region of poleward flow on the western edge of the anticyclone. The vorticity budget is thus qualitatively consistent with a linear Sverdrup balance:

$$\beta \bar{v} \propto \bar{\eta} \frac{\partial \omega}{\partial p}, \quad (13)$$

where β is the planetary vorticity gradient. Thus, transient eddies are a visually prominent feature of the upper-tropospheric response to an asymmetric forcing (e.g., Fig. 13), but they do not prevent the upper-level vorticity from reaching the nonlinear, AMC limit. Instead, vortex squashing produced by the thermally driven ascent is balanced by horizontal advection by the time-mean upper-level anticyclone. This makes the linear scaling of the total vertical mass flux seen for the asymmetric forcings unsurprising, because the overturning circulation is more like that described by the linear model of Gill (1980) than the nonlinear limit of Plumb and Hou (1992). Transient eddies play little role in maintaining high values of absolute vorticity in the heating region. The circulation constraint (3) may be satisfied because there is no local minimum of η in the region of strong divergence, so one cannot draw a closed contour of η locally around the divergent region (e.g., Fig. 13b). Contours of η span all longitudes, and the asymmetric vertical mass flux captured by our metrics may occur in zonal overturnings confined between sets of η contours.

It is important to note that this dynamical regime may be sensitive to the scale of the forcing. Hsu and Plumb (2000) found that transient eddy vorticity fluxes were central to the divergent response created by a forcing that was horizontally narrow compared to the deformation radius and the scale of the resulting anticyclone. Since our asymmetric forcings have the same zonal scale as the resulting anticyclone, this may make stationary eddy fluxes more important here.

4. Summary and discussion

Using a dry, idealized model of Earth’s atmosphere, we investigated the response of the tropical and subtropical tropospheric circulation to off-equatorial thermal forcings localized in both latitude and longitude. This effort was motivated by the fact that previous studies of the nonlinear intensification of meridional flow that occurs when circulations reach AMC states have used either axisymmetric models (e.g., Plumb and Hou 1992; Boos and Emanuel 2008a) or eddy-resolving models with zonally symmetric boundary conditions and forcings (e.g., Schneider and Bordoni 2008). Our work extends a few studies that examined the response to zonally asymmetric forcings (Privé and Plumb 2007b; Hsu and Plumb 2000; Shaw 2014) by examining how the vertical mass flux contained in both zonal and meridional overturnings scales with the strength of the forcing.

Zonally symmetric and asymmetric forcings with the same zonal-mean strength (i.e., the same zonal-mean T_e)

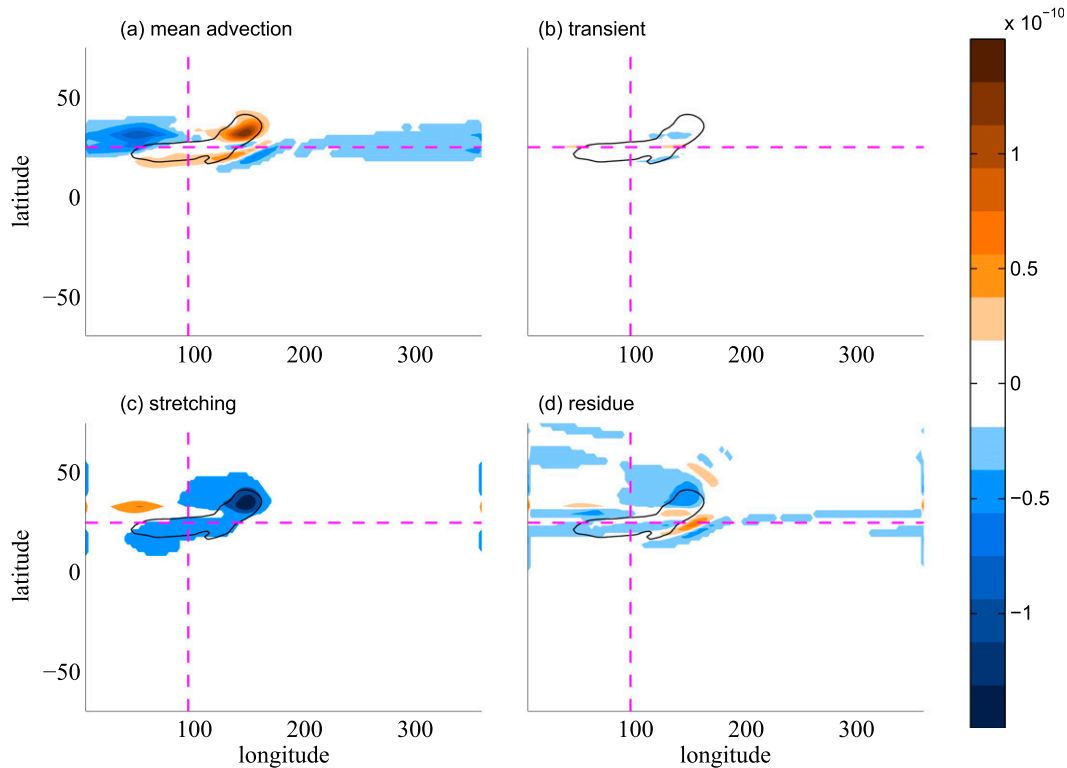


FIG. 15. Components of the vorticity budget (s^{-2}), as in (12), at 200 hPa for the weak zonally asymmetric forcing ($A_e = 12$ K). Labels for each term are as in Fig. 14. The magenta dashed lines mark the latitude and longitude of the equilibrium temperature maximum. The black contour marks upward vertical velocity with 30% of the magnitude of the global maximum upward motion.

produced roughly the same zonal-mean, cross-equatorial Hadley flow and roughly the same minimum value of the zonal-mean upper-tropospheric absolute vorticity. An increase in the sensitivity of the zonal-mean, cross-equatorial mass flux to forcing strength occurred when the off-equatorial, upper-tropospheric absolute vorticity decreased to about half the local value of f , indicating a regime transition of the zonal-mean circulation to an approximate AMC state. For the symmetric forcings, this behavior is consistent with that discussed in previous studies (e.g., Walker and Schneider 2006; Schneider and Bordoni 2008). For the asymmetric forcings, one might expect the zonal-mean value of the forcing to set the zonal-mean response for weak forcings, but it is remarkable that this is also true for strong asymmetric forcings. This might seem at odds with the results of Shaw (2014), who found that a subtropical wavenumber-2 SST anomaly that averaged to zero in the zonal mean substantially increased the strength and meridional extent of a cross-equatorial Hadley cell in an aquaplanet model. However, the cross-equatorial response to the wavenumber-2 forcing in Shaw (2014) was associated with a strong near-equatorial eddy momentum flux divergence created by stationary waves that propagated

from the subtropical forcing across the equator. Our asymmetric forcings create large stationary waves in the subtropics, but these do not propagate into the deep tropics (e.g., Fig. 6b). We speculate that the amplitude of near-equatorial wave activity is greatly enhanced by interaction with moist convection, which is absent in our dry models. Indeed, Boos and Shaw (2013) found that the equatorial wave response to an applied subtropical torque was highly sensitive to the treatment of moist convection in idealized aquaplanet models. More generally, the strength of the zonal-mean, cross-equatorial meridional flow may be highly sensitive to cross-equatorial eddy momentum transports that are only indirectly controlled by subtropical thermal forcings and are sensitive to the details of moist convective coupling with the large-scale flow.

Our most novel result is that the total upward mass flux contained in both zonal and meridional overturnings increases linearly with the strength of the subtropical forcing. This total mass flux is as much as several times larger than the mass flux in the cross-equatorial Hadley cell and exhibits no nonlinear or threshold-like response to the forcing, except for a weakening of its rate of increase at the strongest forcings. These results

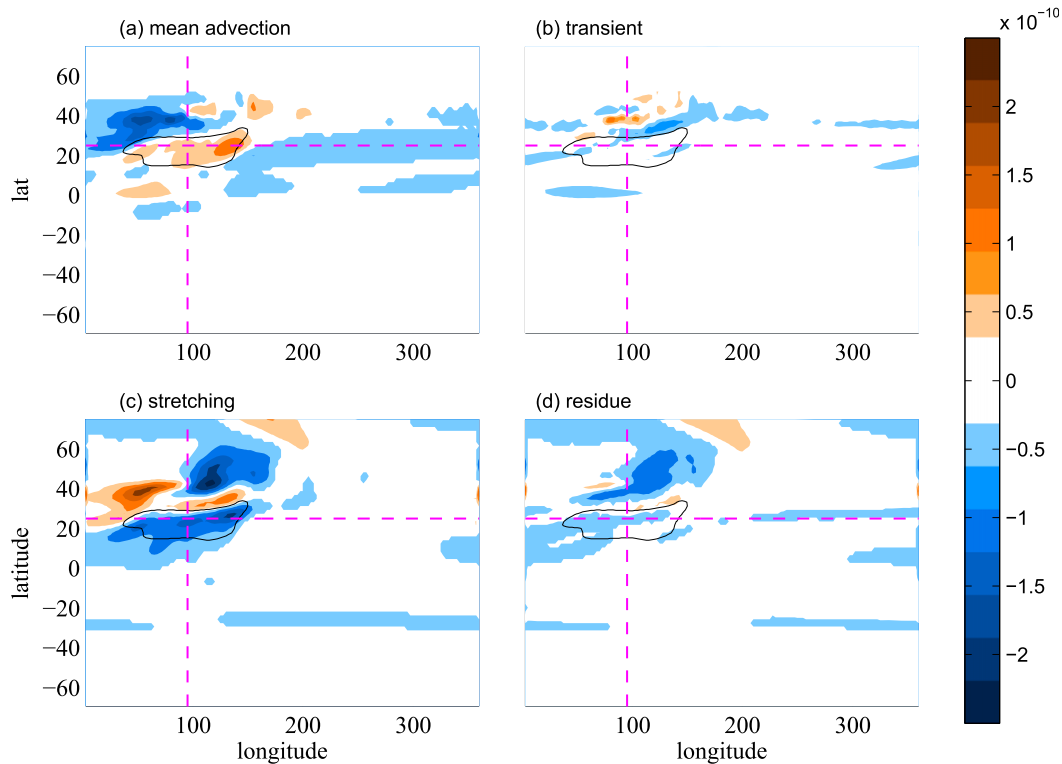


FIG. 16. As in Fig. 15, but for the strong zonally asymmetric forcing ($A_e = 48$ K).

hold whether one includes all upward motions in the measure of the mass flux or whether one includes only the thermally direct ascent. The linear scaling of this total mass flux is accompanied by an upper-tropospheric vorticity balance in which horizontal advection by the time-mean flow compensates for most of the vortex squashing caused by the thermally forced ascent. This means that the dynamics of the total upward mass flux produced by the asymmetric forcing is better described by the Sverdrup balance of the linear model of Gill (1980) than by the nonlinear, AMC regime of Plumb and Hou (1992) or Walker and Schneider (2006). The asymmetric forcing is less effective than the symmetric forcing in reducing the upper-level vorticity toward the nonlinear limit, and it is vorticity advection by time-mean flow rather than transports by transient eddies that provides the largest positive vorticity tendency in the heating region. Although transient eddies are prominent in the upper-tropospheric vorticity field in our models as well as in observations (e.g., Popovic and Plumb 2001), they do not play a dominant role in the vorticity budget in our model. This presents a markedly different view of the dynamical response to a strong subtropical forcing than that presented by Plumb (2007) and motivates a closer examination of observed monsoon circulations in future work. Brief examination of the observations

shown in Fig. 1 shows that the northern branch of the Asian ascent maximum during boreal summer has relatively high vorticities (e.g., near $3 \times 10^{-5} \text{ s}^{-1}$) that may place it in a similar regime to those seen in our model (e.g., compare with the primary ascent maximum in Fig. 13b).

Several important caveats exist. First, in the spirit of Plumb and Hou (1992), our model examined the circulation response to thermal forcings confined to the subtropics. Circulations that are forced by cross-equatorial SST gradients, which often exist in monsoon regions, may be governed by different dynamics. Second, the summer cell in our simulations is too strong compared to the summer cell in Earth's observed solstitial Hadley circulation [e.g., compare Figs. 3b and 3d with the observed mass streamfunctions presented in Dima and Wallace (2003)]. Thus, an overly large fraction of zonal-mean ascent in our model occurs in the summer cell, which might make the total upward mass flux behave more linearly in our models than in the real atmosphere. However, the summer cell in our model strengthens faster than linearly with the strength of the forcing, indicating that its zonal-mean behavior cannot account for the linear scaling of the total upward mass flux. The sublinear scaling needed to offset the nonlinear intensification of the cross-equatorial Hadley cell is seen

only in the zonally asymmetric part of the circulation. Strong zonal overturnings do exist in the northern subtropics during boreal summer, and meridional advection of momentum and vorticity by the upper-tropospheric Asian anticyclone is large even when compared to transports by the zonal-mean flow and transient eddies (e.g., Kelly and Mapes 2013; Shaw 2014). Thus, the overly large strength of the summer cell in our model would not seem to make our results irrelevant to Earth's observed summer circulation.

Our model also lacks moisture and was forced by relaxing temperatures to a prescribed equilibrium distribution. This model design was chosen for consistency with previous influential studies of the Hadley circulation (e.g., Held and Hou 1980; Plumb and Hou 1992), but of course the thermal forcing on Earth arises from surface fluxes of sensible and latent heat that are mixed vertically through the troposphere by dry and moist convection. The large-scale circulation influences this convection as well as the surface enthalpy fluxes, providing a rich set of interactions and potential feedbacks that were omitted from our model. Our prescribed forcings were also constant in time, and it is possible that the time-mean states produced by steady forcings will not be individually realized at each step of a seasonally varying forcing. And as mentioned in the previous section, transient eddy fluxes of vorticity may play a more dominant role in the response to forcings that are zonally narrower than those considered here. Nevertheless, our results raise important questions about how relevant studies of the zonal-mean response to a zonally symmetric forcing are to monsoon circulations, which have large zonal asymmetries in both the forcing and the time-mean responses. The importance of these zonal overturnings for monsoon dynamics merits further examination in both observations and models.

Acknowledgments. Both authors gratefully acknowledge support from National Science Foundation Grant AGS-1253222 and Office of Naval Research Grant N00014-11-1-0617. This work was supported in part by the facilities and staff of the Yale University Faculty of Arts and Sciences High Performance Computing Center. Brian Dobbins provided assistance with model configuration.

REFERENCES

- Boos, W. R., and K. A. Emanuel, 2008a: Wind–evaporation feedback and abrupt seasonal transitions of weak, axisymmetric Hadley circulations. *J. Atmos. Sci.*, **65**, 2194–2214, doi:10.1175/2007JAS2608.1.
- , and —, 2008b: Wind–evaporation feedback and the axisymmetric transition to angular momentum-conserving Hadley flow. *J. Atmos. Sci.*, **65**, 3758–3778, doi:10.1175/2008JAS2791.1.
- , and —, 2009: Annual intensification of the Somali jet in a quasi-equilibrium framework: Observational composites. *Quart. J. Roy. Meteor. Soc.*, **135**, 319–335, doi:10.1002/qj.388.
- , and T. A. Shaw, 2013: The effect of moist convection on the tropospheric response to tropical and subtropical zonally asymmetric torques. *J. Atmos. Sci.*, **70**, 4089–4111, doi:10.1175/JAS-D-13-041.1.
- Bordoni, S., and T. Schneider, 2008: Monsoons as eddy-mediated regime transitions of the tropical overturning circulation. *Nat. Geosci.*, **1**, 515–519, doi:10.1038/ngeo248.
- Dima, I. M., and J. M. Wallace, 2003: On the seasonality of the Hadley cell. *J. Atmos. Sci.*, **60**, 1522–1527, doi:10.1175/1520-0469(2003)060<1522:OTSOTH>2.0.CO;2.
- ECMWF, 2010: ERA-Interim monthly dataset, 1979 to 2010. European Centre for Medium-Range Weather Forecasts, accessed 10 October 2013. [Available online at <http://apps.ecmwf.int/datasets/data/interim-full-mnth/>.]
- Emanuel, K. A., 1995: On thermally direct circulations in moist atmospheres. *J. Atmos. Sci.*, **52**, 1529–1534, doi:10.1175/1520-0469(1995)052<1529:OTDCIM>2.0.CO;2.
- Findlater, J., 1969: Interhemispheric transport of air in the lower troposphere over the western Indian Ocean. *Quart. J. Roy. Meteor. Soc.*, **95**, 400–403, doi:10.1002/qj.49709540412.
- Gill, A., 1980: Some simple solutions for heat-induced tropical circulation. *Quart. J. Roy. Meteor. Soc.*, **106**, 447–462, doi:10.1002/qj.49710644905.
- Haynes, P., and M. McIntyre, 1987: On the evolution of vorticity and potential vorticity in the presence of diabatic heating and frictional or other forces. *J. Atmos. Sci.*, **44**, 828–841, doi:10.1175/1520-0469(1987)044<0828:OTEOVA>2.0.CO;2.
- Held, I., and A. Hou, 1980: Nonlinear axially symmetric circulations in a nearly inviscid atmosphere. *J. Atmos. Sci.*, **37**, 515–533, doi:10.1175/1520-0469(1980)037<0515:NASCIA>2.0.CO;2.
- , and M. Suarez, 1994: A proposal for the intercomparison of the dynamical cores of atmospheric general circulation models. *Bull. Amer. Meteor. Soc.*, **75**, 1825–1830, doi:10.1175/1520-0477(1994)075<1825:APFTIO>2.0.CO;2.
- Hoskins, B. J., and M. J. Rodwell, 1995: A model of the Asian summer monsoon. Part I: The global scale. *J. Atmos. Sci.*, **52**, 1329–1340, doi:10.1175/1520-0469(1995)052<1329:AMOTAS>2.0.CO;2.
- Hsu, C., and R. Plumb, 2000: Nonaxisymmetric thermally driven circulations and upper-tropospheric monsoon dynamics. *J. Atmos. Sci.*, **57**, 1255–1276, doi:10.1175/1520-0469(2000)057<1255:NTDCAU>2.0.CO;2.
- Kelly, P., and B. Mapes, 2011: Zonal mean wind, the Indian monsoon, and July drying in the western Atlantic subtropics. *J. Geophys. Res.*, **116**, D00Q07, doi:10.1029/2010JD015405.
- , and —, 2013: Asian monsoon forcing of subtropical east-erlies in the Community Atmosphere Model: Summer climate implications for the western Atlantic. *J. Climate*, **26**, 2741–2755, doi:10.1175/JCLI-D-12-00339.1.
- Krishnamurti, T. N., P. Ardanuy, Y. Ramanathan, and R. Pasch, 1981: On the onset vortex of the summer monsoon. *Mon. Wea. Rev.*, **109**, 344–363, doi:10.1175/1520-0493(1981)109<0344:OTOVOT>2.0.CO;2.
- Lindzen, R., and A. Hou, 1988: Hadley circulations for zonally averaged heating centered off the equator. *J. Atmos. Sci.*, **45**, 2416–2427, doi:10.1175/1520-0469(1988)045<2416:HCFZAH>2.0.CO;2.
- Murakami, T., L.-X. Chen, and A. Xie, 1986: Relationship among seasonal cycles, low-frequency oscillations, and transient disturbances as revealed from outgoing longwave radiation data. *Mon. Wea. Rev.*, **114**, 1456–1465, doi:10.1175/1520-0493(1986)114<1456:RASCLF>2.0.CO;2.

- Neale, R. B., and Coauthors, 2012: Description of the NCAR Community Atmosphere Model (CAM 5.0). NCAR Tech. Note NCAR/TN-486+STR, 274 pp. [Available online at http://www.cesm.ucar.edu/models/cesm1.0/cam/docs/description/cam5_desc.pdf.]
- Pauluis, O., 2004: Boundary layer dynamics and cross-equatorial Hadley circulation. *J. Atmos. Sci.*, **61**, 1161–1173, doi:10.1175/1520-0469(2004)061<1161:BLDACH>2.0.CO;2.
- Peixoto, J. P., and A. H. Oort, 1992: *Physics of Climate*. American Institute of Physics, 520 pp.
- Plumb, R., 2007: Dynamical constraints on monsoon circulations. *The Global Circulation of the Atmosphere*, T. Schneider and A. H. Sobel, Eds., Princeton University Press, 252–266 pp.
- , and A. Hou, 1992: The response of a zonally symmetric atmosphere to subtropical thermal forcing: Threshold behavior. *J. Atmos. Sci.*, **49**, 1790–1799, doi:10.1175/1520-0469(1992)049<1790:TROAZS>2.0.CO;2.
- Popovic, J., and R. Plumb, 2001: Eddy shedding from the upper-tropospheric Asian monsoon anticyclone. *J. Atmos. Sci.*, **58**, 93–104, doi:10.1175/1520-0469(2001)058<0093:ESFTUT>2.0.CO;2.
- Privé, N. C., and R. A. Plumb, 2007a: Monsoon dynamics with interactive forcing. Part I: Axisymmetric studies. *J. Atmos. Sci.*, **64**, 1417–1430, doi:10.1175/JAS3916.1.
- , and —, 2007b: Monsoon dynamics with interactive forcing. Part II: Impact of eddies and asymmetric geometries. *J. Atmos. Sci.*, **64**, 1431–1442, doi:10.1175/JAS3917.1.
- Rhines, P., 1983: Lectures in geophysical fluid dynamics. *Fluid Dynamics in Astrophysics and Geophysics*, N. R. Lebovitz, Ed., Lectures in Applied Mathematics, Vol. 20, American Mathematical Society, 3–58.
- Schneider, E., 1987: A simplified model of the modified Hadley circulation. *J. Atmos. Sci.*, **44**, 3311–3328, doi:10.1175/1520-0469(1987)044<3311:ASMOTM>2.0.CO;2.
- Schneider, T., 2006: The general circulation of the atmosphere. *Annu. Rev. Earth Planet. Sci.*, **34**, 655–688, doi:10.1146/annurev.earth.34.031405.125144.
- , and S. Bordoni, 2008: Eddy-mediated regime transitions in the seasonal cycle of a Hadley circulation and implications for monsoon dynamics. *J. Atmos. Sci.*, **65**, 915–934, doi:10.1175/2007JAS2415.1.
- , P. O’Gorman, and X. Levine, 2010: Water vapor and the dynamics of climate changes. *Rev. Geophys.*, **48**, RG3001, doi:10.1029/2009RG000302.
- Shaw, T. A., 2014: On the role of planetary-scale waves in the abrupt seasonal transition of the Northern Hemisphere general circulation. *J. Atmos. Sci.*, **71**, 1724–1746, doi:10.1175/JAS-D-13-0137.1.
- Sobel, A., and R. Plumb, 1999: Quantitative diagnostics of mixing in a shallow water model of the stratosphere. *J. Atmos. Sci.*, **56**, 2811–2829, doi:10.1175/1520-0469(1999)056<2811:QDOMIA>2.0.CO;2.
- , and C. Bretherton, 2000: Modeling tropical precipitation in a single column. *J. Climate*, **13**, 4378–4392, doi:10.1175/1520-0442(2000)013<4378:MTPIAS>2.0.CO;2.
- Walker, C. C., and T. Schneider, 2005: Response of idealized Hadley circulations to seasonally varying heating. *Geophys. Res. Lett.*, **32**, L06813, doi:10.1029/2004GL022304.
- , and —, 2006: Eddy influences on Hadley circulations: Simulations with an idealized GCM. *J. Atmos. Sci.*, **63**, 3333–3360, doi:10.1175/JAS3821.1.
- Webster, P. J., 1972: Response of the tropical atmosphere to local, steady forcing. *Mon. Wea. Rev.*, **100**, 518–541, doi:10.1175/1520-0493(1972)100<0518:ROTTAT>2.3.CO;2.
- , and J. Fasullo, 2003: Monsoon: Dynamical theory. *Encyclopedia of Atmospheric Sciences*, J. A. Curry and J. A. Pyle, Eds., Elsevier Science Ltd., 1370–1386, doi:10.1016/B0-12-227090-8/00236-0.
- Yin, M. T., 1949: Synoptic-aerologic study of the onset of the summer monsoon over India and Burma. *J. Atmos. Sci.*, **6**, 393–400, doi:10.1175/1520-0469(1949)006<0393:SASOTO>2.0.CO;2.
- Zheng, X., and E. A. Eltahir, 1998: The role of vegetation in the dynamics of West African monsoons. *J. Climate*, **11**, 2078–2096, doi:10.1175/1520-0442-11.8.2078.